Electrically controlled layer-dependent localized spin flipping in Janus CrSTe

Liyenda Gogoi and Pritam Deb*

Advanced Functional Materials Laboratory, Department of Physics, Tezpur University (Central University), Tezpur 784028, India

(Received 27 July 2023; revised 21 October 2023; accepted 8 May 2024; published 28 May 2024)

Localized control of magnetism is one of the fundamental aspects in the development of spintronic applications. In this article, we report the observation of electrically controllable layer-dependent unique magnetization reversal in the ferromagnetic Janus van der Waals material CrSTe with robust perpendicular magnetic anisotropy. We propose an electrical shielding mechanism based on charge and spin redistribution in the system that modulates the localized spin flipping restricted to a single magnetic layer. These observations demonstrate the possibility of a purely electrically controllable, compact, low-power-consuming spintronic device consisting of a few atomic layers of a single material.

DOI: 10.1103/PhysRevB.109.174439

I. INTRODUCTION

Switching magnetic ordering using electric effects is highly desirable for advanced spintronic devices, particularly in magnetically active data storage devices. Application of magnetic field is the conventional technique to achieve spin flipping in magnetic material. However, this technique consumes high power. Alternatively, electric-field-based spin manipulation is a potential replacement and has been implemented by modulating the interfacial magnetoelectric coupling [1] and reversing the Dzyaloshinskii-Moriya interaction (DMI) chirality by voltage pulse [2]. Electrical control of magnetism reduces the consumption of energy, enhances the storage capacity, and hosts a rapid data reading-writing process that leads to higher performance of spintronic devices [1,3–5]. However, these approaches utilized to switch the global magnetization, or magnetization of specific components of a heterostructure, cannot be used for localized spin switching in a single material. In modern spintronics, to fabricate compact devices, layer-dependent control of magnetism is required. To achieve such localized modulation, materials that exhibit layer-dependent variation of properties are required. Transition metal chalcogenide (TMC) materials belonging to the van der Waals (vdW) family provide a suitable platform to tailor magnetism and related phenomena via different mechanisms [6–14]. The presence of strong spin-orbit coupling in these materials enables the magnetoelectric effect. With well-defined spin projections, layered vdW structures, and ease of integration, TMCs become viable contenders for spintronic applications [15,16]. Nonetheless, the presence of out-of-plane symmetry and absence of DMI impede the full utilization of TMCs in spintronics. Additionally, inversion symmetry and the centrosymmetric nature of TMCs is a barrier to achieving higher magnetic moments, Curie temperatures, and localized physical properties [17–21]. By breaking the out-of-plane symmetry in TMCs, these barriers are eliminated, which enables spin manipulation.

Creating structurally asymmetric Janus materials having distinct surfaces with different components on each side offers a crucial approach to breaking mirror symmetry in TMCs [22–28]. This asymmetry enables localized tailored magnetic characteristics on a single nanostructure, thereby facilitating layer-dependent variation of magnetism which is beneficial for high-density data storage, rapid read-write operations, and efficient spintronic applications [29,30]. For such rapid, compact, low-power-consuming spintronic advancement, few-layered Janus materials with strong electrical modulating flexibility are crucial.

In this article, we investigate the magnetic properties of Janus CrSTe under electric influence. The CrSTe Janus structure is expected to demonstrate favorable electrical adjustability due to the adaptable magnetic behavior and magnetoelectric coupling in its parent systems CrS_2 [31–34] and $CrTe_2$ [35–38]. $CrTe_2$ switches magnetic anisotropy based on stacking and layer number [35], and CrS_2 shows phase transitions via electrostatic doping [34]. Here, we have investigated the magnetoelectric coupling in Janus CrSTe. It possesses strong magnetic anisotropy and facilitates a unique controllable layer-specific magnetization reversal through electrical means, which has not been reported earlier to the best of our knowledge. We also propose an electrically driven magnetization reversal mechanism rooted in charge redistribution and consequential electric shielding.

II. COMPUTATIONAL METHODS

Our first-principles calculations were performed using density functional theory (DFT) with the projector augmented wave method implemented in Quantum Espresso [39,40]. The exchange correlation effects are calculated within the generalized gradient approximation of Perdew-Burke-Ernzerhof form [41–43]. A plane wave basis set with a 90 Ry cutoff energy is employed. Brillouin zone integration utilized a $32 \times 32 \times 32$ k mesh. Grimme's DFT-D2 method provides vdW correction

*Corresponding author: pdeb@tezu.ernet.in

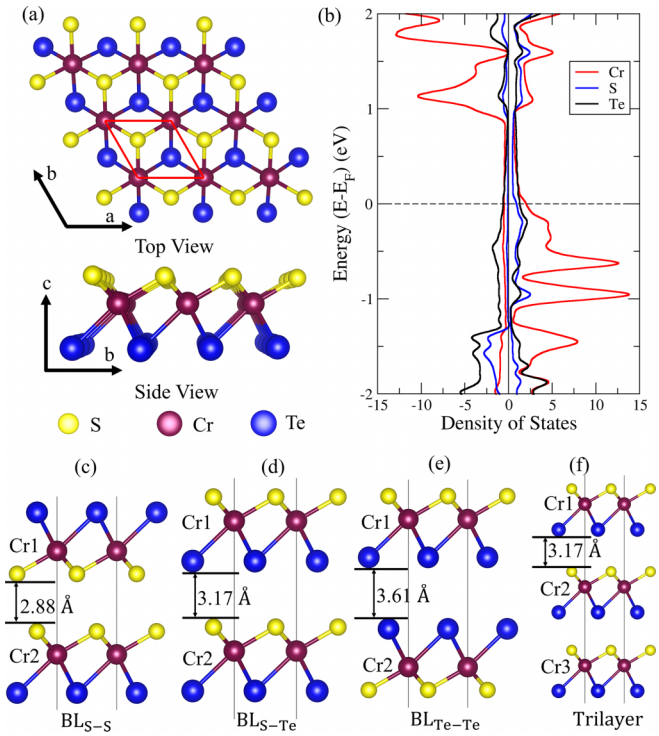

FIG. 1. Optimized structures and electronic properties. (a) Top and side views of CrSTe monolayer. The red rhombus represents the unit cell. (b) PDOS of monolayer CrSTe. (c)–(f) Three bilayers having S-S, S-Te, and Te-Te atoms in the interface, respectively, and the trilayer system.

[44]. The 15 Å along the z axis prevented periodic image interaction. Energy convergence criterion is set to 10^{-10} Ry. Magnetoelectric effects are studied by considering spin-orbit coupling.

III. RESULTS AND DISCUSSION

The optimized Janus CrSTe monolayer where the transition metal atom Cr is sandwiched between two chalcogen atoms S and Te is illustrated in Fig. 1(a). Geometric optimization reveals that the most stable configuration is attained with a unit cell where $a = b = 3.45$ Å, which is in good agreement with existing literature [45,46]. The optimized lattice parameter for the Janus CrSTe falls between those of CrS_2 and $CrTe_2$ [47]. There are no imaginary frequencies in the phonon dispersion, which demonstrates the dynamical stability of the system. The phonon dispersion of the system is shown in the Supplemental Material (Fig. S1) [48]. The chemical stability of CrSTe is evaluated by calculating cohesive energy using the formula $E_{coh} = (E_{Cr} + E_S + E_{Te} - E_{CrSTe})/3$ where E_{CrSTe}, E_{Cr}, E_S, and E_{Te} are the energy of the 2D CrSTe unit cell and isolated atoms of Cr, S, and Te, respectively [49]. The cohesive energy of CrSTe is $E_{coh} = 3.72$ eV/atom, which favors the formation of CrSTe from the binary analog.

Figure 1(b) illustrates the system's magnetically active and electrically conductive characteristics through the spin-polarized projected density of states. The intrinsic electric potential difference arising due to Janus structure implies differing behavior on different sides under electrical perturbation. Moreover, the Janus structure's diverse elemental composition allows for multiple bilayer stacking possibilities, leading to three distinct bilayers of CrSTe denoted as BL$_{S-S}$, BL$_{S-Te}$, and BL$_{Te-Te}$ (with S-S, S-Te, and Te-Te interfacial atoms, respectively) as shown in Figs. 1(c)–1(e). Optimized structural parameters are depicted in the respective Figs. 1(c)–1(e).

The Janus monolayer displays a ferromagnetic (FM) ground state, determined through exchange energy calculations. The process of calculation of exchange energy is shown in the Supplemental Material (Fig. S2, Sec. II) [48]. Although the presence of structural asymmetry introduces the Dzyaloshinskii-Moriya interaction (DMI) into a system, a report suggests that the DMI in this system is not sufficient to affect the ferromagnetic ground state of Janus CrSTe [45]. Moreover, our micromagnetic simulation of the ground state of the magnetic atoms in the Janus CrSTe monolayer also reveals that the system is ferromagnetic in nature. The spin texture of the monolayer Janus CrSTe is shown in the Supplemental Material (Fig. S3). In this system, central Cr atoms are the primary magnetic contributors, with a local magnetic moment of 2.35 μ_B. In contrast, chalcogen atoms S and Te exhibit negligible local magnetic moments and are antiferromagnetically coupled to Cr. Thus, Cr dominates the spin polarization [Fig. 1(b)]. Exchange energy calculations also confirm ferromagnetic interlayer magnetic orientations across all bilayer systems as depicted in the Supplemental Material (Table I) [48].

Magnetic anisotropy is a critical factor dictating the stability of magnetic orientation in 2D materials, which is quantified by magnetic anisotropic energy (MAE). This energy reflects the effort needed in the transition of magnetic moments between the easy axis and hard axis of magnetization. Greater MAE values correlate with heightened 2D magnetic stability. Our investigation delves into the magnetic anisotropy of monolayer CrSTe and its bilayer systems. Variation of MAE with polar and azimuthal angle is represented in the Supplemental Material (Fig. S4) [48]. By exploring how MAE evolves with polar and azimuthal angles, we determine that monolayer CrSTe displays a perpendicular magnetic anisotropy (PMA) with an easy axis of magnetization. Bilayer systems also exhibit PMA with varying strengths. Calculation yield MAE values of 6.647 meV/nm^2, 11.071 meV/nm^2, 8.33 meV/nm^2, and 11.87 meV/nm^2 for monolayer, BL$_{S-S}$, BL$_{S-Te}$, and BL$_{Te-Te}$, respectively. The monolayer's significantly elevated MAE, compared to CrS_2 and $CrTe_2$ [33], facilitated greater magnetic stability and a higher Curie temperature (303 K) in the Janus CrSTe. The calculation of Curie temperature is depicted in the Supplemental Material (Fig. S5, Sec. V) [48]. Furthermore, bilayer formation enhances MAE and thus strengthen the ferromagnetic properties in stacked CrSTe bilayers.

Controlling magnetic ordering in low-dimensional materials is pivotal for spintronic applications. To achieve a low-power-consuming spin-flipping mechanism in Janus materials for efficient spintronics, we explore CrSTe's response to an electric field, because electrically driven spin modulation consumes far less power than traditional magnetic reading and writing methods. Electric fields are simulated in positive

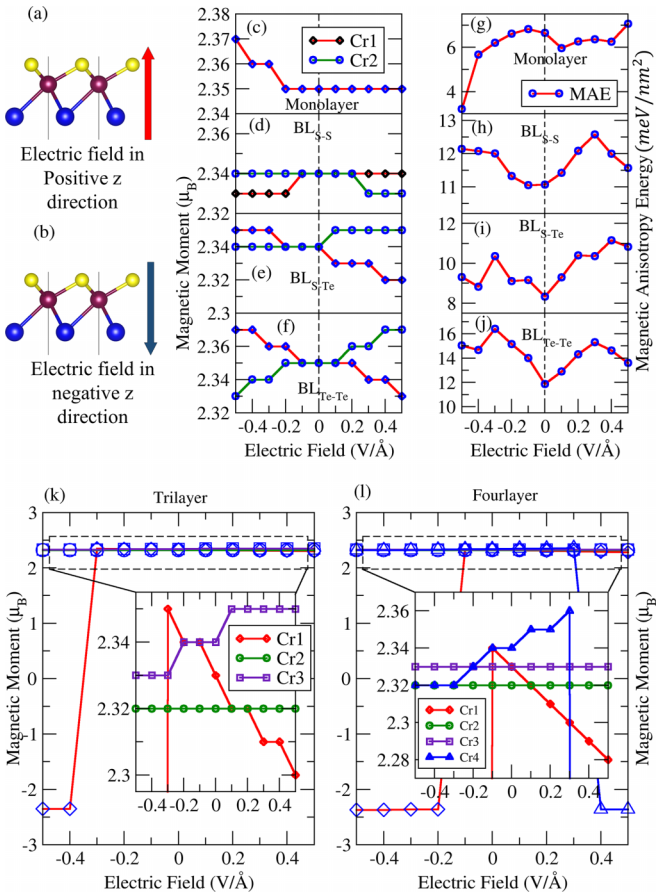

FIG. 2. Variation of magnetic properties with electric field. (a), (b) Application of perpendicular electric field in positive and negative z directions. The red and blue arrows represent the direction of electric field. (c)–(f) Magnetic moment variation of Cr atoms in monolayer, BL_{S-S}, BL_{S-Te}, and BL_{Te-Te} with electric field. (g)–(j) Variation of MAE of monolayer, BL_{S-S}, BL_{S-Te}, and BL_{Te-Te} with electric field. (k), (l) Variation of magnetic moment of Cr atoms of trilayer and four-layer systems. The inset shows an enlarged view of the magnetic moment variation.

and negative z directions as shown in Figs. 2(a) and 2(b) to examine magnetic modulation in the designed systems. Electric field magnitudes range from ± 0.1 V/Å to ± 0.5 V/Å. Application of an electric field to the CrSTe Janus monolayer induces changes in magnetic moment. Under positive z direction of electric fields, directed toward the S atom, the Cr atom's magnetic moment remains constant despite increasing electric field strength. Conversely, the magnetic moment gradually increases under negative bias as the electric field strength rises. This variation of magnetic moments is shown in Fig. 2(c).

Figure 2(c) illustrates the anisotropic nature of magnetic moment variation with electric fields in the monolayer. In one electric field polarity, the magnetic moment remains steady, while in the other, it changes. Bilayer systems also exhibit intriguing behaviors when their magnetic characteristics are assessed in the presence of electric fields. Figure 2(d) depicts magnetic moment variation in BL_{S-S}, where Cr magnetic moments mostly remain constant, displaying only minimal changes. In BL_{S-Te} [Fig. 2(e)], under positive electric fields, the upper Cr atom's (Cr1) magnetic moment gradually decreases, while the other Cr atom's (Cr2) magnetic moments remain nearly constant, except for a small initial enhancement. Under negative biasing, both Cr atoms' magnetic moments remain constant. Figure 2(f) outlines the magnetic moment profile of BL_{Te-Te}, revealing that the two Cr atoms' magnetic moments respond in opposite directions to changing electric fields in the two biasing modes. These magnetic moment variations underscore distinct magnetic behaviors of Cr atoms based on their locations within the system.

Furthermore, the MAE of the studied systems also changes with varying electric fields as illustrated in Figs. 2(g)–2(j). Figure 2(g) displays the MAE variation of the monolayer CrSTe with electric field. Notably, MAE remains relatively constant under positive biasing and gradually decreases under negative biasing. Intriguingly, despite these variations, the magnetic orientation consistently remains perpendicular across the entire range of applied field, emphasizing the robustness of the PMA in the CrSTe monolayer. Additionally, the MAE variation across all bilayer systems is favorable for application purposes. Their MAE increases with electric field, signifying enhanced ferromagnetic stability. This strengthened resistance of PMA to electrical perturbation makes this system a strong contender for electric field-driven applications.

Collectively, the figures and analyses reveal signatures of layer-dependent variation of magnetism. In certain systems, specific Cr atoms' magnetic behavior remains impervious to electric fields. This prompts us to propose a hypothesis that during electric field application, a mechanism shields these particular Cr atoms from electric effects. To validate this proposition, we explore more extended S-Te interface structures involving three and four layers of CrSTe. Trilayer and four-layer systems adopting S-S and Te-Te stacking arrangements are omitted due to symmetric magnetic moment variations under opposite electric field biasing, as our focus rests on asymmetric variations of magnetism. The trilayer structure is depicted in Fig. 1(f), while the four-layer system is presented in the Supplemental Material (Fig. S6) [48]. Magnetic moment data for the trilayer and four-layer systems under positive and negative electric biases show that Cr atoms positioned within the systems (Cr2 for trilayer, Cr2 and Cr3 for four-layer) remain unaffected by electric fields. This observation substantiates the presence of a shielding effect upon electric field application. Figures 2(k) and 2(l) highlight unique behaviors in magnetic moment variation for the trilayer and four-layer systems. Remarkably, the magnetic moment of the upper Cr layer (Cr1) changes magnetic alignment after reaching a specific electric field value (-0.3 V/Å for trilayer and -0.2 V/Å for four-layer). Furthermore, the bottom Cr atoms (Cr4) in the four-layer system shift magnetic orientation after 0.3 V/Å of electric field. This discovery is particularly intriguing in our study. The observed magnetization reversal signifies a transition from interlayer ferromagnetic to antiferromagnetic alignment in specified magnetic layers in trilayer and four-layer systems. This transition of magnetic alignment is also evident in the variation of interlayer magnetic exchange energy with electric field as shown in the Supplemental Material (Table II)

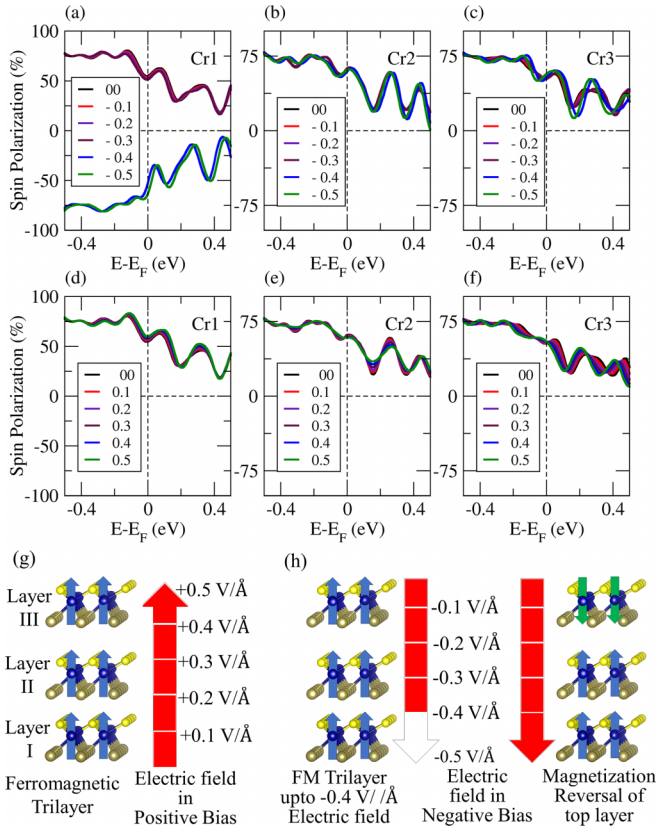

FIG. 3. Variation of localized spin polarization. Variation of spin polarization percentage of Cr1, Cr2, Cr3 with negative [(a)–(c)] and positive [(d)–(f)] electric bias in trilayer. (g), (h) Schematic representation of the unaltered magnetic orientation and magnetization reversal in trilayer under positive and negative bias of electric field, respectively. Blue/green arrows represent up/down magnetic orientation.

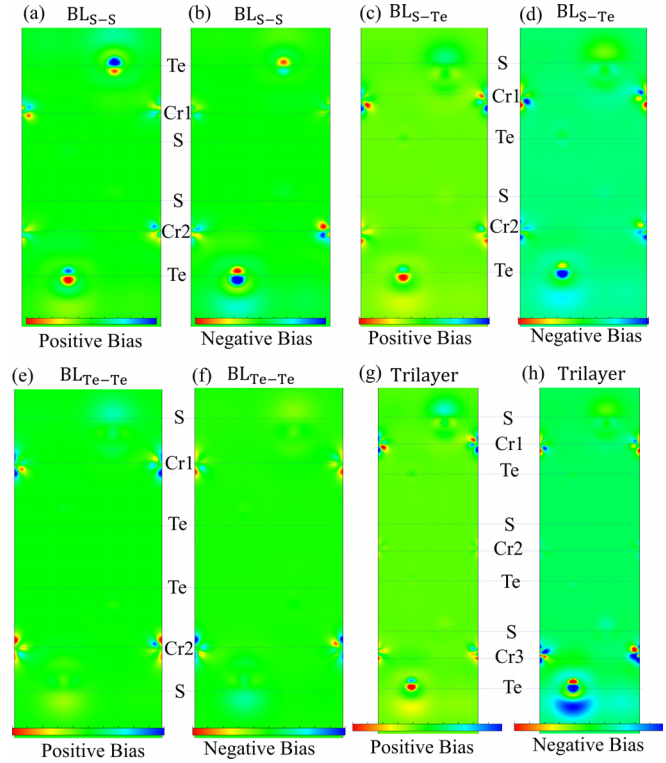

FIG. 4. Charge redistribution profile of bilayers and trilayer under electric field. (a)–(h) Charge redistribution BL$_{S-S}$, BL$_{S-Te}$, BL$_{Te-Te}$, and trilayer under positive and negative bias. The red end and blue end of the scale represent charge accumulation and charge depletion, respectively. Positions of the atoms are shown by dotted line.

[48]. In the trilayer system, change of sign in exchange energy value from positive to negative signifies the transition from interlayer ferromagnetic to interlayer antiferromagnetic alignment of magnetic moments. Interestingly, the interlayer exchange constant J_{23} between the Cr2 and Cr3 layers is not much affected by electric field while J_{12} between Cr1 and Cr2 changes significantly and changes sign under application of electric field as depicted in the Supplemental Material (Table III). From this variation of interlayer exchange constant, it is evident that the layer-dependent variation of interlayer exchange constant leads to spin flipping in the system. Hence, the profound magnetization reversal in the multilayerd system arises from the spin-polarized electron spin flipping under electric field as shown in Figs. 3(a)–3(f). However, this reversal is confined solely to a single surface layer, as the other interior layers remain unaffected by electric fields due to the proposed shielding mechanism. Importantly, this magnetic reversal transpires under negative biasing in the trilayer and under both biasings in the four-layer system.

Figure 3 illustrates the atomically resolved spin polarization percentage variation of Cr atoms within the trilayer system under both electric biasings. These figures distinctly reveal that local spin polarization of the Cr1 atom [Fig. 3(a)] flips from positive to negative after an applied electric field of -0.4 V/Å, while the spin polarization of the other two Cr atoms remains positive. Intriguingly, there is no spin polarization flip under positive bias. This outcome is schematically depicted in Figs. 3(g) and 3(h). Figure 3(g) portrays unchanged magnetic orientation across all three layers under the entire range of applied positive bias, while Fig. 3(h) illustrates the magnetization switch in the upper layer after -0.4 V/Å of negative electric bias. Furthermore, Figs. 3(a)–3(f) showcase substantial spin polarization variations in certain Cr atoms (Cr3 in both biases and Cr1 under negative bias). Conversely, electric effects minimally impact spin polarization in other Cr atoms (Cr2).

The distinctive layer-dependent variations in magnetic properties have prompted the concept of a shielding effect emerging under electric fields. To validate this concept and understand observed behavior, we explore charge redistribution profiles in the studied systems. Figures 4(c) and 4(d) show charge redistribution in BL$_{S-Te}$ under a ± 0.5 V/Å electric field in positive and negative biases. Notably, substantial charge redistribution occurs at Te surface sites and the farthest Cr atom from the Te site. In contrast, atoms inside these two extremities and the S atom on extreme surfaces remain unaffected. Te exhibits more significant charge redistribution than S due to its lower electronegativity compared to S. Figures 4(a)–4(b) and Figs. 4(e)–4(f) depict charge redistribution in BL$_{S-S}$ and BL$_{Te-Te}$ bilayers under positive

and negative electric biases. In BL_{S-S}, charge redistribution predominantly occurs around Te surface atoms, effectively shielding inner atoms. This results in relatively constant magnetic moments for both Cr atoms [Fig. 2(d)]. Conversely, in BL_{Te-Te}, the surface S atom fails to shield against electric field effects, while charges around Cr atoms just beneath it redistribute and shield interior atoms. This leads to gradual magnetic moment changes [Fig. 2(e)] in BL_{Te-Te}. A similar charge redistribution profile is observed for the trilayer [Figs. 4(g) and 4(h)] and four-layer system as shown in the Supplemental Material (Fig. S6) [48]. Notably, electric field does not affect charge distribution in middle-layer Cr atoms.

Our analysis of magnetic moment variations and charge redistribution profiles reveals that electrically induced charge redistribution triggers a shielding effect within the Janus system. When the applied electric field is pointed toward the Te surface, charge depletion takes place at Te sites, and charge accumulates at the farthest side from the Te site. This results in an electrostatic potential difference between Te sites and the opposite extreme site. This potential difference generates an intrinsic electric field that counteracts the applied field's effects. Similar effects occur when the electric bias is reversed. Our observations indicate that the magnetic moment of Cr atoms is enhanced/suppressed where charge accumulates/depletes under the influence of electric field. Furthermore, Te atoms on the surface shield electric field effects, whereas S atoms lack this behavior, regardless of their location or exposure to electric perturbation. This shielding property ensures minimal impact on magnetic moment of Cr atoms positioned just below Te atoms and greater influence on magnetic moment of Cr atoms at the S side.

The observed magnetization reversal specifically occurs in Cr atoms where charge accumulation is witnessed. This selective reversal in magnetization, confined to a solitary surface layer, aligns with the charge redistribution mechanism. Our analysis indicates that the electric field's impact is counteracted solely by the redistributed charges around the surface Te atom and the distant Cr atoms. In cases where charges around Te atoms are redistributed, there is slight charge redistribution around Cr atoms positioned just below those surface Te atoms. However, no charge redistribution is observed in interior Cr atoms. Consequently, solely the Cr atoms engaged in either shielding or sharing charges with surface Te atoms experience spin polarization flipping. This mechanism underpins the intriguing layer-dependent magnetization reversal in both the trilayer and four-layer Janus structures.

This intriguing discovery of electrically controllable transitions between interlayer ferromagnetic and antiferromagnetic phases in Janus materials holds significant promise for spintronic applications. This Janus system stands as a strong candidate for magnetic tunneling junctions (MTJs). In a multilayered structure, one of the Janus layers can be substituted by a magnetically inactive electrical insulator and magnetic orientation of one of the magnetic layers could be flipped between FM and AFM coupling with the other layer by applying an external electric bias. In this way, by switching the electric field on and off, the MTJ can switch between high and low resistance states, presenting a novel approach to writing a magnetic state. This underscores the potential application of our multilayer hybrid Janus system in spintronic devices.

IV. CONCLUSION

In summary, our study reveals an electrically driven, layer-dependent, localized magnetization reversal mechanism facilitated by shielding through charge redistribution in Janus CrSTe. This technique of localized magnetization switching holds significant promise in advancing single-material-based spintronics. The confinement of spin flipping to a single layer of Cr atoms, coupled with the nondestructive, robust perpendicular magnetic anisotropy (PMA) observed in multilayer stacking under electric fields, positions Janus materials as formidable contenders for advanced, compact, and low-power-consuming spintronic devices with a few atomic layers' thickness.

ACKNOWLEDGMENTS

We acknowledge the Indian Institute of Technology, Kharagpur, for providing supercomputing facilities under the National Supercomputing Mission (NSM), Government of India. L.G. sincerely thanks Dr. M. Bora, S. Mohanty, and A. K. Singh for productive scientific discussions.

[1] J. T. Heron, M. Trassin, K. Ashraf, M. Gajek, Q. He, S. Y. Yang, D. E. Nikonov, Y.-H. Chu, S. Salahuddin, and R. Ramesh, Electric-field-induced magnetization reversal in a ferromagnet-multiferroic heterostructure, Phys. Rev. Lett. **107**, 217202 (2011).

[2] D. Yu, Y. Ga, J. Liang, C. Jia, and H. Yang, Voltage-controlled Dzyaloshinskii-Moriya interaction torque switching of perpendicular magnetization, Phys. Rev. Lett. **130**, 056701 (2023).

[3] K. F. Mak, J. Shan, and D. C. Ralph, Probing and controlling magnetic states in 2D layered magnetic materials, Nat. Rev. Phys. **1**, 646 (2019).

[4] R. Yoshimi, K. Yasuda, A. Tsukazaki, K. Takahashi, M. Kawasaki, and Y. Tokura, Current-driven magnetization switching in ferromagnetic bulk Rashba semiconductor (Ge,Mn)Te, Sci. Adv. **4**, eaat9989 (2018).

[5] G. Assefa, Electric field controlled itinerant carrier spin polarization in ferromagnetic semiconductors, Adv. Condens. Matter Phys. **2021**, 1 (2021).

[6] M. Bora, S. Mohanty, A. Singh, W. Gao, and P. Deb, Adaptive half-metallicity via magnetic proximity in an electrically sensitive 1T'-WTe_2/$CrBr_3$ vdW heterostructure, Appl. Surf. Sci. **623**, 157019 (2023).

[7] B. L. Chittari, D. Lee, N. Banerjee, A. H. MacDonald, E. Hwang, and J. Jung, Carrier-and strain-tunable intrinsic magnetism in two-dimensional MAX_3 transition metal chalcogenides, Phys. Rev. B **101**, 085415 (2020).

[8] L. Gogoi, W. Gao, P. M. Ajayan, and P. Deb, Quantum magnetic phenomena in engineered heterointerface of low-dimensional van der Waals and non–van der Waals materials, Phys. Chem. Chem. Phys. **25**, 1430 (2023).

[9] Y. Guo, J. Dai, J. Zhao, C. Wu, D. Li, L. Zhang, W. Ning, M. Tian, X. C. Zeng, and Y. Xie, Large negative magnetoresistance induced by anionic solid solutions in two-dimensional spin-frustrated transition metal chalcogenides, Phys. Rev. Lett. **113**, 157202 (2014).

[10] M. Bora, S. K. Behera, P. Samal, and P. Deb, Magnetic proximity induced valley-contrasting quantum anomalous Hall effect in a graphene-$CrBr_3$ van der Waals heterostructure, Phys. Rev. B **105**, 235422 (2022).

[11] X. Yao, L. Wang, Y. Sun, X. Li, J. Sun, B. Wang, M. He, and X. Zhang, Two-dimensional transition metal triborides: Monolayers with robust intrinsic magnetism and high spin stability, Phys. Rev. B **105**, 214421 (2022).

[12] S. K. Behera and P. Deb, Spin-transfer-torque mediated quantum magnetotransport in MoS_2/phosphorene vdW heterostructure based MTJs, Phys. Chem. Chem. Phys. **22**, 19139 (2020).

[13] P. Li, Q. Cui, Y. Ga, J. Liang, and H. Yang, Large Dzyaloshinskii-Moriya interaction and field-free topological chiral spin states in two-dimensional alkali-based chromium chalcogenides, Phys. Rev. B **106**, 024419 (2022).

[14] S. K. Behera, M. Bora, S. S. P. Chowdhury, and P. Deb, Proximity effects in graphene and ferromagnetic $CrBr_3$ van der Waals heterostructures, Phys. Chem. Chem. Phys. **21**, 25788 (2019).

[15] N. Zibouche, A. Kuc, J. Musfeldt, and T. Heine, Transition-metal dichalcogenides for spintronic applications, Ann. Phys. (Berlin, Ger.) **526**, 395 (2014).

[16] L. Cao, X. Deng, G. Zhou, S.-J. Liang, C. V. Nguyen, L. K. Ang, and Y. S. Ang, Multiferroic van der Waals heterostructure $FeCl_2/Sc_2CO_2$: Nonvolatile electrically switchable electronic and spintronic properties, Phys. Rev. B **105**, 165302 (2022).

[17] J. Liang, W. Wang, H. Du, A. Hallal, K. Garcia, M. Chshiev, A. Fert, and H. Yang, Very large Dzyaloshinskii-Moriya interaction in two-dimensional Janus manganese dichalcogenides and its application to realize skyrmion states, Phys. Rev. B **101**, 184401 (2020).

[18] I. Dzyaloshinsky, A thermodynamic theory of "weak" ferromagnetism of antiferromagnetics, J. Phys. Chem. Solids **4**, 241 (1958).

[19] T. Moriya, New mechanism of anisotropic superexchange interaction, Phys. Rev. Lett. **4**, 228 (1960).

[20] Z. Shao, J. Liang, Q. Cui, M. Chshiev, A. Fert, T. Zhou, and H. Yang, Multiferroic materials based on transition-metal dichalcogenides: Potential platform for reversible control of Dzyaloshinskii-Moriya interaction and skyrmion via electric field, Phys. Rev. B **105**, 174404 (2022).

[21] Y. Chen, Q. Fan, Y. Liu, and G. Yao, Electrically tunable magnetism and unique intralayer charge transfer in Janus monolayer MnSSe for spintronics applications, Phys. Rev. B **105**, 195410 (2022).

[22] A.-Y. Lu, H. Zhu, J. Xiao, C.-P. Chuu, Y. Han, M.-H. Chiu, C.-C. Cheng, C.-W. Yang, K.-H. Wei, Y. Yang *et al.*, Janus monolayers of transition metal dichalcogenides, Nat. Nanotechnol. **12**, 744 (2017).

[23] J. Zhang, S. Jia, I. Kholmanov, L. Dong, D. Er, W. Chen, H. Guo, Z. Jin, V. B. Shenoy, L. Shi *et al.*, Janus monolayer transition-metal dichalcogenides, ACS Nano **11**, 8192 (2017).

[24] C. Xia, W. Xiong, J. Du, T. Wang, Y. Peng, and J. Li, Universality of electronic characteristics and photocatalyst applications in the two-dimensional Janus transition metal dichalcogenides, Phys. Rev. B **98**, 165424 (2018).

[25] S. Ji, R. Yao, C. Quan, J. Yang, F. Caruso, and X. Li, Anomalous valley Hall effect induced by mirror symmetry breaking in transition metal dichalcogenides, Phys. Rev. B **107**, 174434 (2023).

[26] W. Qiao, S. Yan, Y. Hu, C. Zhao, S. Gao, R. Bai, and T. Zhou, Two-dimensional ferromagnetism with strong magnetic interactions induced by Janus-type hydrogenation in $FeSe_2$, Phys. Rev. B **107**, 184419 (2023).

[27] M. Angeli, G. R. Schleder, and E. Kaxiras, Twistronics of Janus transition metal dichalcogenide bilayers, Phys. Rev. B **106**, 235159 (2022).

[28] N. Ghobadi, S. G. Rudi, and S. Soleimani-Amiri, Electronic, spintronic, and piezoelectric properties of new Janus ZnAXY (A = Si, Ge, Sn, and X, Y = S, Se, Te) monolayers, Phys. Rev. B **107**, 075443 (2023).

[29] R. Li, J. Jiang, X. Shi, W. Mi, and H. Bai, Two-dimensional Janus FeXY (X, Y = Cl, Br, and I, X ≠ Y) monolayers: Half-metallic ferromagnets with tunable magnetic properties under strain, ACS Appl. Mater. Interfaces **13**, 38897 (2021).

[30] D. Dey and A. S. Botana, Structural, electronic, and magnetic properties of vanadium-based Janus dichalcogenide monolayers: A first-principles study, Phys. Rev. Mater. **4**, 074002 (2020).

[31] K. Chen, J. Deng, Y. Yan, Q. Shi, T. Chang, X. Ding, J. Sun, S. Yang, and J. Z. Liu, Diverse electronic and magnetic properties of CrS_2 enabling strain-controlled 2D lateral heterostructure spintronic devices, npj Comput. Mater. **7**, 79 (2021).

[32] X.-H. Tian and J.-M. Zhang, First-principles prediction of the structural, electronic, and magnetic properties of nonmetal atoms doped single-layer CrS_2, Phys. Status Solidi B **256**, 1900149 (2019).

[33] G. Xiao, W.-Z. Xiao, Q. Chen, and L.-l. Wang, Novel two-dimensional ferromagnetic materials CrX_2 (X = O, S, Se) with high Curie temperature, J. Mater. Chem. C **10**, 17665 (2022).

[34] C. Wang, X. Zhou, Y. Pan, J. Qiao, X. Kong, C.-C. Kaun, and W. Ji, Layer and doping tunable ferromagnetic order in two-dimensional CrS_2 layers, Phys. Rev. B **97**, 245409 (2018).

[35] Y. Liu, S. Kwon, G. J. de Coster, R. K. Lake, and M. R. Neupane, Structural, electronic, and magnetic properties of $CrTe_2$, Phys. Rev. Mater. **6**, 084004 (2022).

[36] X. Zhang, Q. Lu, W. Liu, W. Niu, J. Sun, J. Cook, M. Vaninger, P. F. Miceli, D. J. Singh, S.-W. Lian *et al.*, Room-temperature intrinsic ferromagnetism in epitaxial $CrTe_2$ ultrathin films, Nat. Commun. **12**, 2492 (2021).

[37] N. Abuawwad, M. dos S. Dias, H. Abusara, and S. Lounis, Noncollinear magnetism in two-dimensional $CrTe_2$, J. Phys.: Condens. Matter **34**, 454001 (2022).

[38] A. Purbawati, S. Sarkar, S. Pairis, M. Kostka, A. Hadj-Azzem, D. Dufeu, P. Singh, D. Bourgault, M. Nuñez-Regueiro, J. Vogel *et al.*, Stability of the in-plane room temperature van der Waals ferromagnet chromium ditelluride and its conversion to chromium-interleaved $CrTe_2$ compounds, ACS Appl. Electron. Mater. **5**, 764 (2023).

[39] P. Giannozzi, S. Baroni, N. Bonini, M. Calandra, R. Car, C. Cavazzoni, D. Ceresoli, G. L. Chiarotti, M. Cococcioni, I. Dabo *et al.*, QUANTUM ESPRESSO: a modular and open-source software project for quantum simulations of materials, J. Phys.: Condens. Matter **21**, 395502 (2009).

[40] P. Giannozzi, Jr., O. Andreussi, T. Brumme, O. Bunau, M. B. Nardelli, M. Calandra, R. Car, C. Cavazzoni, D. Ceresoli, M. Cococcioni *et al.*, Advanced capabilities for materials modelling with Quantum ESPRESSO, J. Phys.: Condens. Matter **29**, 465901 (2017).

[41] M. Ernzerhof and G. E. Scuseria, Assessment of the Perdew-Burke-Ernzerhof exchange-correlation functional, J. Chem. Phys. **110**, 5029 (1999).

[42] Y. Wang and J. P. Perdew, Correlation hole of the spin-polarized electron gas, with exact small-wave-vector and high-density scaling, Phys. Rev. B **44**, 13298 (1991).

[43] G. Kresse and D. Joubert, From ultrasoft pseudopotentials to the projector augmented-wave method, Phys. Rev. B **59**, 1758 (1999).

[44] S. Grimme, Semiempirical GGA-type density functional constructed with a long-range dispersion correction, J. Comput. Chem. **27**, 1787 (2006).

[45] Q. Cui, J. Liang, Z. Shao, P. Cui, and H. Yang, Strain-tunable ferromagnetism and chiral spin textures in two-dimensional Janus chromium dichalcogenides, Phys. Rev. B **102**, 094425 (2020).

[46] Q.-Q. Li, W.-W. Liu, Z.-K. Ding, H. Pan, X.-H. Cao, W.-H. Xiao, N.-N. Luo, J. Zeng, L.-M. Tang, B. Li, K.-Q. Chen, and X.-D. Duan, Stacking- and strain-dependent magnetism in Janus CrSTe bilayer, Appl. Phys. Lett. **122**, 121902 (2023).

[47] C. M. O. Bastos, R. Besse, J. L. F. Da Silva, and G. M. Sipahi, *Ab initio* investigation of structural stability and exfoliation energies in transition metal dichalcogenides based on Ti-, V-, and Mo-group elements, Phys. Rev. Mater. **3**, 044002 (2019).

[48] See Supplemental Material at http://link.aps.org/supplemental/10.1103/PhysRevB.109.174439 for more details about (1) Phonon spectrum of monolayer and bilayer CrSTe, (2) Calculation of magnetic anisotropy energy and magnetic configuration stability, (3) Spin texture of monolayer CrSTe, (4) Variation of MAE with polar and azimuthal angle, (5) Curie temperature of CrSTe, (6) Charge redistribution of fourlayer system under applied electric field, and (7) Interlayer exchange energy of trilayer CrSTe.

[49] A. Kandemir and H. Sahin, Janus single layers of In_2SSe: A first-principles study, Phys. Rev. B **97**, 155410 (2018).